Membrane-Aerated Biofilm Proton and Oxygen Flux during Chemical Toxin Exposure

E. S. MCLAMORE,*,[†],[‡],[§] W. ZHANG,[†],[‡]
D. M. PORTERFIELD,[†],[§],[‖] AND
M. K. BANKS[†],[‡]

Bindley Bioscience Center and Birck Nanotechnology Center, Discovery Park: Physiological Sensing Facility, School of Civil Engineering, Department of Agricultural & Biological Engineering, and Department of Horticulture & Landscape Architecture, Purdue University. 1203 West State Street, West Lafayette, Indiana 47907-2057

Bioreactors containing sessile bacteria (biofilms) grown on hollow fiber membranes have been used for treatment of many wastestreams. Real time operational control of bioreactor performance requires detailed knowledge of the relationship between bulk liquid water quality and physiological transport at the biofilm–liquid interface. Although large data sets exist describing membrane-aerated bioreactor effluent quality, very little real time data is available characterizing boundary layer transport under physiological conditions. A noninvasive, microsensor technique was used to quantify real time ($\approx$1.5 s) changes in oxygen and proton flux for mature *Nitrosomonas europaea* and *Pseudomonas aeruginosa* biofilms in membrane-aerated bioreactors following exposure to environmental toxins. Stress response was characterized during exposure to toxins with known mode of action (chlorocarbonyl cyanide phenyl-hydrazone and potassium cyanide), and four environmental toxins (rotenone, 2,4-dinitrophenol, cadmium chloride, and pentachlorophenol). Exposure to sublethal concentrations of all environmental toxins caused significant increases in O_2 and/ or H^+ flux (depending on the mode of action). These real time microscale signatures (i.e., fingerprints) of O_2 and H^+ flux can be coupled with bulk liquid analysis to improve our understanding of physiology in counter-diffusion biofilms found within membrane aerated bioreactors; leading to enhanced monitoring/modeling strategies for bioreactor control.

Introduction

Sessile growth of bacteria (biofilms) occurs throughout the aquatic environment. Sessile bacteria are embedded within extracellular polymers which provides protection against environmental stress (*1*) (e.g., UV radiation (*2*) and chemical toxin exposure (*3*)). In addition, biofilm formation has many unique protective advantages over planktonic growth, including metabolically diverse microniche formation (*4*), and community-based transfer of genetic information (*5*). There are many approaches for engineering reactors designed to promote the growth of biofilms, and reactor type is often driven by wastestream composition, cost, and available footprint. Membrane aerated bioreactors (MABR) are a viable technology for many environmental applications, including: nitrification (*6*), combined nitrification/denitrificaiton (*7, 8*), and degradation of various organics (*9–11*); also see the review in ref *12*.

On line measurement of bioreactor effluent water quality has recently been proposed for enhancing bioreactor performance (*13, 14*). Operational decisions based on real time measurements require detailed knowledge of the relationship between bulk liquid water quality and physiological transport at the biofilm-liquid interface (i.e., boundary layer). Bulk liquid and boundary layer physiological characterizations have been conducted for biofilms grown on nonporous surfaces using a variety of techniques (*15–18*). This large set of data has improved the accuracy of engineering assumptions for design, control, and modeling of biofilm reactors (*19, 20*). Physiology of biofilms in MABRs (counter diffusion of oxygen) is significantly different than biofilms grown on nonporous material (i.e., codiffusion) (*21*), and to date there is very little real time data describing boundary layer transport.

Here, we use an advanced microsensor technique known as self-referencing (SR) for noninvasive in situ measurement of MABR biofilm boundary layer H^+ and O_2 transport under stressed and nonstressed conditions. SR (see the review in ref *22*) is a technique that has been used for decades in biomedical (*23*) and agricultural (*24*) applications, and has recently been adopted for environmental applications (*25, 26*). The technique filters noise not associated with bioactive transport by computer controlled oscillation of microsensors according to Fick's first law of diffusion: $J = D(\Delta C/\Delta X)$, where J = analyte flux, D = molecular diffusion constant, C = analyte concentration, and X = diffusionary distance. SR induces a phase dependent output signal where the amplitude is proportional to the differential analyte concentration (ΔC) measured over the oscillation distance (ΔX) (*22–26*). This significant improvement in signal-to-noise ratio is critical to microscale measurements, as electrochemical sensors with an active surface area smaller than 1 mm are subject to "antenna noise" due to electromagnetic interferences (*27*). Flux was measured for nitrifying and chemoorganoheterotrophic biofilms during exposure to (i) chemicals with known mode of toxic action and (ii) four common environmental toxins which are known to cause oxidative stress. In situ characterization of oxidative stress response mechanisms will improve our understanding of real time physiological transport, and can be coupled with currently available bulk liquid data for improving control strategies and dynamic simulations.

Experimental Section

The chemolithoautotrophic nitrifying bacteria *Nitrosomonas europaea* (Winogradsky) was used as a model organism to study the effect of chemical toxin exposure since this organism has relatively few defense mechanisms (*28*). *Pseudomonas aeruginosa* (PA01) was used as a model chemoorganoheterotrophic sessile bacteria with a wide array of defense mechanisms (*29*). *N. europaea* and *P. aeruginosa* biofilms (American Type Culture Collection (ATCC), Manassas, VA) were grown in straight tube, upflow membrane aerated bioreactors (MABR) within environmental growth chambers (25 and 38 °C, respectively) at a transmembrane

* Corresponding author phone: (806)239-9556; e-mail: emclamor@purdue.edu.
[†] Physiological Sensing Facility.
[‡] School of Civil Engineering.
[§] Department of Agricultural & Biological Engineering.
[‖] Department of Horticulture & Landscape Architecture.

pressure of 25 kPa (*26, 30*). During the first 30 days, the free stream velocity was 0.5 cm sec^{-1} ($Re = 60$) to allow formation of a homogeneous, mature biofilm. After maturation, the free stream velocity was reduced to 0.01 m sec^{-1}, ($Re = 3.1$) and biofilms were then allowed to grow under laminar flow conditions for 30 days. *N. europaea* biofilms were grown in ATCC medium 2265 with a pH of 7.7 ± 0.2 (NH$_4^+$ as primary electron donor) and *P. aeruginosa* biofilms were grown in ATCC medium 1065 LB medium with 10 mM TRIS buffer (pH 7.4 ± 0.1). All physiological flux experiments were conducted following at least 30 days of steady state growth under laminar conditions. Steady state growth was based on less than a 5% change in bulk liquid effluent chemical oxygen demand, dissolved oxygen concentration, and pH (see Supporting Information (SI) Table S1). Biofilm thickness was measured using a high resolution Pulnix progressive scan camera (JAI, Inc., San Jose, CA) with an Optem 70XL zoomscope (Fairport, NY) and a National Instruments frame grabber (Austin, TX). The flowcell containing a fixed silicone membrane was positioned on a vibration isolation table (Technical Manufacturing Corporation, Peabody, MA) (camera was in horizontal position). The location of the biofilm surface was recorded using the framegrabber at 10 locations along each biofilm. Thickness was measured at various radial locations by rotating the membrane 90°. Biofilm thickness was calculated by subtracting the average vertical position of the bare membrane from the position of the biofilm surface, and values averaged for three replicate biofilm samples.

Sensor Construction. Fiber optic oxygen microsensors (optrodes) used a frequency domain lifetime fluorometer and were constructed using previously published techniques (*31, 32*). Optrodes (5–7 μm tip diameter) were calibrated in sterile, nitrogen purged growth media, and O$_2$ saturated growth media (21%). Measured phase angle was transduced to an analog signal via a digital signal processor (World Precision Instruments, Sarasota, FL) (*25, 33*). Proton-selective microelectrodes (2–5 μm tip diameter) were constructed following published procedures (*34*), and calibrated using both standard pH buffers (Sigma Aldrich, St. Louis, MO), and sterile growth media in the 4–8 pH range (media pH was adjusted by titrating with 1 MHCl/NaOH). Measured potential was recorded at 1kHz against a Ag/AgCl reference electrode (3 M KCl and 3% agar) (*34*).

Physiological Flux. Physiological oxygen and proton flux were measured using self-referencing microsensors (*25, 33*) (SI Figure S1). To validate the use of SR microsensors under physiological conditions, O$_2$/H$^+$ flux microprofiles were first measured within the mass boundary layer formed at the fluid-biofilm interface for both *N. europaea* and *P. aeruginosa* biofilms (*26*). Silicon membranes with intact biofilms were extracted from bioreactors, transferred to flow cells, and allowed to stabilize for 30 min under continuous flow at 0.01 m sec^{-1} ($Re = 3.1$) (*26*). Analyte flux was measured within the mass boundary layer, and microprofiles were compared to first order Fickian diffusion models; the correlation coefficient between the predicted and measured data was reported as the dynamic efficiency (ε) (*26, 22*). Based on these microprofiles, the distance of the mass boundary layer (δ) for each biofilm was calculated using published techniques (*26*).

To correct for underestimation of extracellular proton transport in buffered media, a post measurement correction technique was used (*34*). For the *N. europaea* growth, the total buffer concentration and pK_a values used were 47 mM, and 7.2, respectively; for *P. aeruginosa* growth media, these values were 50 mM, and 8.2, respectively (pK_a determined by acid/base titration).

Experimental Section. For pre and postexposure steady state values, microsensors were positioned at the surface (within 2 μm) of each biofilm using the camera-zoomscope

and linear stepper motors (*22, 24, 26*). Flux was recorded at six locations along the surface of each replicate biofilm, and average steady state values calculated by averaging each measurement (error bars represent standard error of the arithmetic mean). Steady state flux was defined as less than a 3% change in $\Delta C/\Delta X$ for nine consecutive flux recordings (*26*). After measuring surface flux, chemical toxin(s) were added to an injection port upstream of the flowcell using a pipet; free stream velocity during all experiments was 0.01 m sec^{-1} ($Re = 3.1$). When applicable, subsequent chemical additions were made after observing steady state flux. As a control experiment, sterile growth media was added while flux continuously recorded following the same methods. All experiments were repeated for five replicate biofilm samples to ensure validity of physiological trends.

N. europaea and *P. aeruginosa* biofilms were first exposed to compounds with known mode of toxic action (MOA): chlorocarbonyl cyanide phenyl-hydrazone (CCCP), and potassium cyanide (KCN). CCCP (Acros Organics, West Chester, PA) uncouples oxidative phosphorylation from electron transport (increasing oxygen and proton flux) (*35*). At high concentrations, KCN (Sigma Aldrich, St. Louis, MO) blocks electron transport, reduces viability, and can cause cell lysis in unacclimated cells (reducing proton and oxygen flux).

Four environmental contaminants were chosen that vary in MOA, but are known to directly affect aerobic respiration: rotenone, 2,4-dinitrophenol (DNP), cadmium chloride (CdCl$_2$), and pentachlorophenol (PCP) (Sigma Aldrich). Rotenone has been used as an insecticide and pesticide, is associated with neurological disorders in humans, and can inhibit electron transfer by preventing NADH-ATP conversion; (decreasing oxygen flux) (*36*). Rotenone test concentrations (25–50 μM) were based on previously published values using SR optrodes (*25*). DNP is an uncoupler of oxidative phosphorylation with a similar MOA as CCCP, and has been associated with neurological and endocrine-disrupting effects (*37*). Concentration of DNP (Sigma Aldrich, St. Louis, MO) in the environment is highly variable, and is a function of various physicochemical properties. Therefore, the concentrations tested were based on preliminary experiments and were identical to concentrations used for CCCP experiments (20–40 μM). Cadmium is a persistent environmental contaminant which effects DNA repair, phospholipid regulation, respiration, and has been reported to stimulate production of reactive oxygen species (*38*) (altering H$^+$ and O$_2$ transport). CdCl$_2$ concentrations (1–10 μM) were based on previous research using planktonic bacteria *N. europaea* (*39*). PCP (Sigma Aldrich, St. Louis, MO) has been shown to have uncoupling effects, and also has been shown to cause oxidative stress (altering both H$^+$ and O$_2$ flux) (*29, 40*). PCP concentrations (1–10 μM) were based on the 24 h human health advisory level (*41*). All stock solutions of PCP were prepared in a 0.1% dimethyl sulfoxide solution.

Confocal microscopy was used to characterize viability following exposure to control drugs (CCCP and KCN) using a membrane integrity stain (BacLight Live/Dead viability kit; Invitrogen Molecular Probes, Carlsbad, CA). SYTO9 (green) was used to stain intact cells, and propidium iodide (red) was used to stain cells with compromised membranes (1:1 ratio). For all experiments, 3 μL of stain was added to 1.5 mL of PBS, samples immersed for 20 min, and then rinsed in PBS prior to imaging. A Zeiss LSM 710 (Thornwood, NY) confocal microscope with multiwavelength lasers (488 and 514 nm) was used for excitation, and Zen software (Zeiss, Thornwood, NY) was used for image capture and orthogonal image processing (Version 1.43f, NIH Image). Five cross sections of 144 μm by 144 μm were analyzed over a total biofilm depth of 128 μm (2 μm sections) using a 10× objective lens.
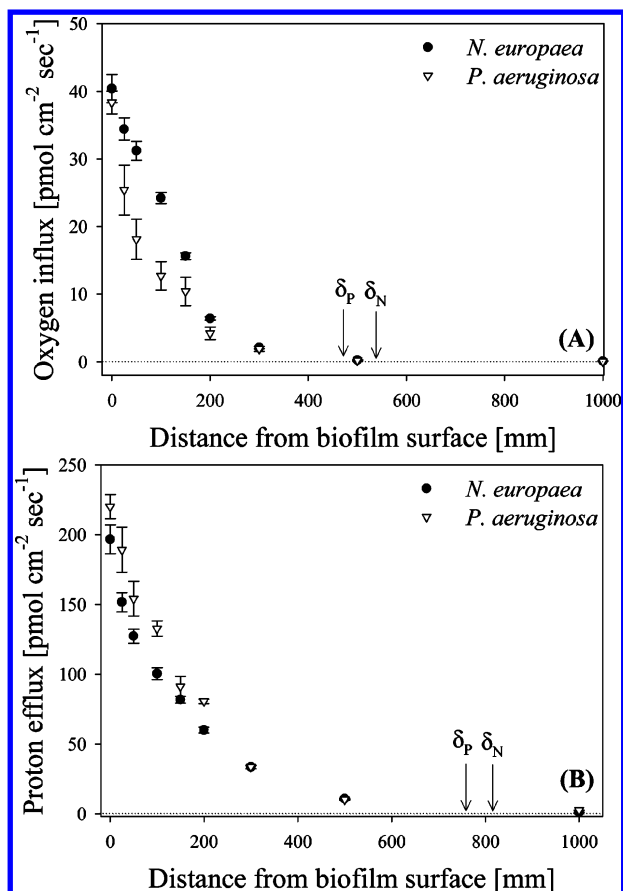
FIGURE 1. Representative plot of (A) oxygen and (B) proton flux within the biofilm-liquid mass boundary layer formed near the surface of *N. europaea* and *P. aeruginosa* biofilms. Average mass boundary layer thickness (δ) is indicated on the plot for each species (subscript denotes species type).

Statistical Analysis. Mean percent change in O_2/H^+ flux was calculated by averaging continuous flux measurements for at least 2 min during pre-exposure, peak exposure, and post exposure measurements. Analysis of variance (ANOVA) was used to test for significant differences ($\alpha = 0.05$) between flux values for each condition. All reported error bars for SR data represent one standard error of the arithmetic mean.

Results

Oxygen and proton microsensors were calibrated and characterized (detection limit, response time, sensitivity), and sensor performance did not deviate from previously published results (*33, 34*). Oxygen and proton flux within 2 mm of *N. europaea* and *P. aeruginosa* biofilm surfaces was measured, and the distance of the mass boundary layer (δ) calculated (*26*). The value of δ for *N. europaea* oxygen ($529 \pm 21\ \mu m$) and proton flux ($816 \pm 18\ \mu m$) was significantly larger than *P. aeruginosa* oxygen ($481 \pm 15\ \mu m$) and proton flux ($760 \pm 19\ \mu m$) ($p < 0.01$, $\alpha = 0.05$, $n = 5$; Figure 1). *N. europaea* boundary layer thickness for O_2 was near values previously reported for the substrate: NH_4^+ ($470 \pm 21\ \mu m$), and byproduct: NO_2^- ($585 \pm 33\ \mu m$) transport (*26*), although the H^+ boundary layer was significantly larger (reflected by the significantly larger diffusion coefficient for H^+). The correlation between measured and predicted values (ε) based on an empirical transport model (*22, 23, 26*) was >0.98 for all biofilms ($n = 5$). Measured δ values for each biofilm were within the range ($200-1000\ \mu m$) of previously reported values using microelectrodes (*42-45*). In addition to validating the use of the SR technique for noninvasively quantifying transport, accurate characterization of chemical gradients formed near the biofilm-liquid interface is extremely useful for modeling/monitoring applications (*13, 14, 19, 20*). All subsequent real time measurements of $\Delta C/\Delta X$ were measured within $1-2\ \mu m$ of the biofilm surface (where maximum bulk liquid-biofilm transport occurs).

Chemical Toxin Exposure and Stress Response. A representative plot of *N. europaea* O_2/H^+ flux during exposure to compounds with known MOA (CCCP and KCN) is shown in Figure 2 (for average data over the biofilm surface, see Figure 4). After a short period required for diffusion into the biofilm (1.6 ± 0.2 min), CCCP ($20\ \mu M$) caused a significant increase in oxygen influx (pre-exposure: 34 ± 5 pmol cm^{-2} s^{-1}; peak stress response: 61 ± 3 pmol cm^{-2} s^{-1}). A concurrent increase in active proton efflux occurred (pre and peak flux values were 102 ± 2 pmol cm^{-2} s^{-1}, and 1440 ± 183 pmol cm^{-2} s^{-1}). In preliminary experiments O_2/H^+ flux values returned to near-basal levels after an average of 15 ± 0.2 min. This oxidative stress response is a result of increased H^+ permeability across the cytoplasmic membrane due to the uncoupling action of CCCP. This increased transport does not lead to an increase in ATPase activity, and is thus known as uncoupling of electron transport from ATP production
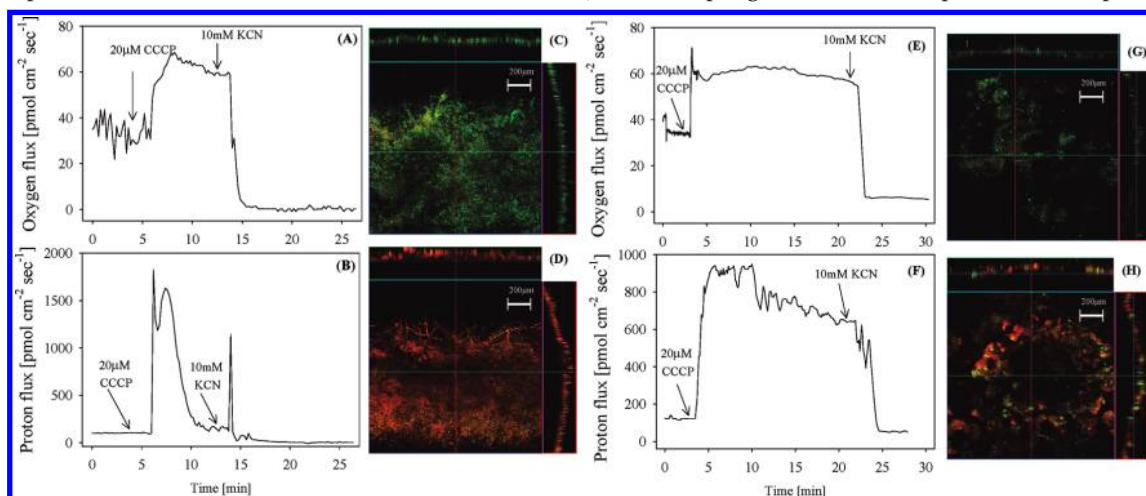
FIGURE 2. (A) *N. europaea* biofilm oxygen flux and (B) proton flux during exposure to 20 μM CCCP and 10 mM KCN. (C) Representative confocal image of *N. europaea* biofilm (grown for 30 days) on a silicone membrane. (D) Representative image of *N. europaea* biofilm 30 min after exposure to 20 μM CCCP and 10 mM KCN. (E) *P. aeruginosa* biofilm oxygen flux and (F) proton flux during exposure to 20 μM CCCP and 10 mM KCN. (G) Representative confocal image of *P. aeruginosa* biofilm (grown for 30 days), and (H) image of *P. aeruginosa* biofilm 30 min after exposure to 10 mM KCN. Images were taken at a depth of 50 μm, and the three-dimensional image is shown in orthogonal view, which depicts the surface of the hollow fiber silicone membrane.

(*35, 46, 47*). Subsequent addition of 10 mM KCN inhibited respiration after an average of 3.2 min, indicated by reduced O_2 and H^+ flux to 0.5 ± 0.4 pmol cm^{-2} s^{-1}, and 2.4 ± 3.5 pmol cm^{-2} s^{-1}, respectively. No significant flux was noted after 30 min of exposure to 20 μM CCCP and 10 mM KCN, indicating that cell viability was significantly reduced (O_2/H^+ flux were 1.6 ± 0.4 pmol cm^{-2} s^{-1} and 0.6 ± 0.2 pmol cm^{-2} s^{-1}, respectively). This was validated using a membrane-permeability stain. Orthogonal confocal images show intact cells throughout the biofilm matrix before exposure to toxins (Figure 2C), and cells with damaged membranes following exposure to CCCP/KCN (Figure 2D). The right orthogonal images depict full penetration of the dye and excitation laser to the surface of the hollow fiber silicone membrane. Low resolution (10×) images were used to ascertain viability/membrane integrity of the entire biofilm (rather than utilizing single cell spatial resolution).

Representative proton/oxygen flux for *P. aeruginosa* biofilms exposed to CCCP and KCN is shown in Figure 2E and F. Similar to *N. europaea*, uncoupling was observed following a 1.7 ± 0.3 min diffusion time. Steady state O_2 flux increased from 34.2 ± 0.7 pmol cm^{-2} s^{-1} to 57.9 ± 0.9 pmol cm^{-2} s^{-1} following addition of 20 μM CCCP, and decreased to 6.0 ± 0.8 pmol cm^{-2} s^{-1} following addition of 10 mM KCN. Proton flux increased from 122.9 ± 7.6 pmol cm^{-2} s^{-1} to 655.2 ± 30.2 pmol cm^{-2} s^{-1} following addition of 20 μM CCCP, and decreased to 91.8 ± 5.8 pmol cm^{-2} s^{-1} following addition of 10 mM KCN, indicating a significant decrease in viability; validated using a membrane integrity stain (Figures 2G and H). The observed trends in O_2/H^+ flux following exposure to chemicals with known MOA were used as a baseline comparison for understanding O_2/H^+ flux during exposure to environmental toxins.

Figure 3A demonstrates representative bulk liquid pH and O_2 concentration during exposure of *P. aeruginosa* biofilms to 5 μM CdCl$_2$ (measured in the effluent of the flowcell). A minimum of 4 h was required to detect significant changes in bulk liquid pH (−0.5) and oxygen concentration (+16.5 μM). However, measurement of biophysical H^+ and O_2 flux at the surface of *P. aeruginosa* biofilms revealed an increase in O_2/H^+ flux following a 3.3 ± 0.2 min period required for diffusion of CdCl$_2$ into the biofilm (noted as "*diff*" on Figure 3B). This immediate physiological response (noted as "*peak*" in Figure 3B) is due to a combination of stress response mechanisms, likely including efflux pumping, oxidative stress, ion homeostasis, and uncoupling of oxidative phosphorylation. After an average of 7.3 ± 0.2 min, the peak in O_2/H^+ flux decreased (noted as "*post*" in Figure 3B), although both oxygen and proton flux were significantly higher than preexposure levels (50 ± 4% for O_2 and 87 ± 20% for H^+). Postexposure flux remained for up to 12 h in replicate experiments. This difference in signals from real time measurements of bulk liquid and boundary layer pH/O_2 is attributed to the amount of time required for changes in metabolic transport to effect bulk liquid composition relative to background noise and/or concentration drift. Representative images of real time H^+/O_2 flux during exposure to rotenone, DNP and PCP are presented in SI Figure S2.

Using the approach demonstrated in Figure 3, the percent change in flux during peak O_2/H^+ flux, and steady state post exposure for *N. europaea* and *P. aeruginosa* biofilms (n = five replicate biofilms) was calculated during exposure to rotenone, DNP, CdCl$_2$, and PCP (Figure 4). To account for spatial heterogeneity, six surface flux measurements were recorded for each biofilm (separated by a distance of 1 mm). All physiological stress responses were significantly greater than null controls (addition of sterile growth media). After addition of rotenone, DNP, CdCl$_2$, and PCP, surface pH (6.8 ± 0.2) and O_2 concentration (144 ± 24 μM) did not significantly differ relative to pre-exposure levels for either species during the 20
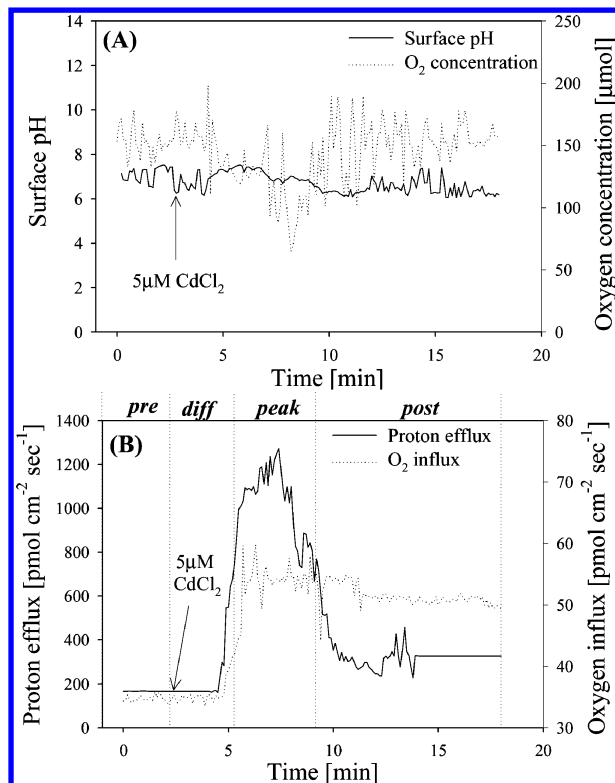
FIGURE 3. Representative plot demonstrating *N. europaea* proton and oxygen flux (A) surface pH and O_2 concentration during exposure to 5 μM CdCl$_2$ for a *P. aeruginosa* biofilm (grown for 30 days). (B) Real time H^+ and O_2 flux for *P. aeruginosa* biofilm exposed to 5 μM CdCl$_2$ (indicated by arrow). Time periods associated with steady state pre-exposure (*pre*), toxin diffusion (*diff*), peak stress response (*peak*), and steady state postexposure (*post*) are indicated.

min allotted for the experiments ($p < 0.025$, $\alpha = 0.05$), but changed significantly after a minimum of 4 h.

For both species of biofilm, boundary layer O_2/H^+ flux significantly increased following exposure to 20−40 μM CCCP (positive control), but returned to near basal levels after an average of 35 ± 0.2 min. Proton flux was more affected by exposure to CCCP than O_2 flux, which is attributed to the MOA of the proton ionophore (*47*). Exposure to 10 mM KCN (negative control) reduced O_2/H^+ flux by 92−98% for both species, indicating a significant reduction of cell viability (dormancy of *P. aeruginosa* cannot be ruled out based on these results).

Rotenone (25−50 μM) caused a temporary increase (peak stress response) in O_2 influx, but had only a small effect on peak H^+ flux. After 8−10 min, O_2 flux returned to near basal levels (<3% change). Based on the known MOA (*36*), this change in O_2 flux was due to inhibition of NADH-ATP conversion.

DNP (20−40 μM) caused uncoupling effects which were not statistically different from CCCP ($p = 0.02$, $\alpha = 0.05$). Proton flux was more significantly affected than O_2 flux for both species of biofilm. This result is not surprising, as in addition to being an environmental toxin, DNP is also used as an uncoupler in pharmacology experiments (*47*).

At the lowest concentration tested (5 μM), CdCl$_2$ significantly increased O_2/H^+ flux for both species, and flux reduced to levels which were significantly greater than basal levels (indicative of sublethal oxidative stress and/or reduced viability). Uncoupling was increased for 50 μM CdCl$_2$, and for *N. europaea* this concentration caused a decrease in O_2 flux by 29 ± 4%. This reduction in aerobic respiration was not observed for *P. aeruginosa* exposed to 50 μM CdCl$_2$,
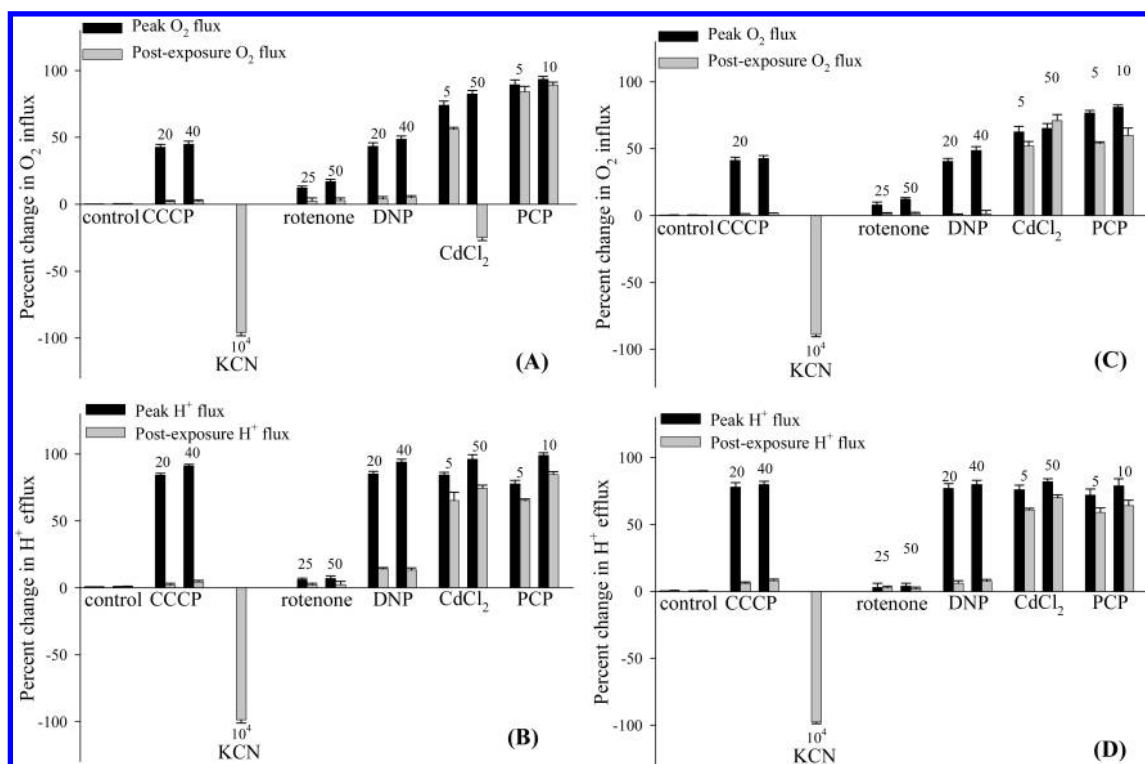
FIGURE 4. Average change in (A) oxygen and (B) proton flux for *N. europaea* following exposure to environmental toxins. Plots represent calculated average flux at six positions along the biofilm surface separated by distance of 1 mm (n = five replicate biofilms), and error bars represent standard error of the arithmetic mean. Average (C) oxygen and (B) proton flux for *P. aeruginosa* biofilms (n = 5) exposed to environmental toxins. Peak physiological response and postexposure steady state (as previously defined) are indicated in each plot. All numbers represent toxin concentration (uM) added after at least 30 min of steady state O_2 and H^+ flux.

although O_2/H^+ flux was increased by $98 \pm 0.9\%$, indicating significant oxidative stress.

PCP caused the most significant increase in O_2/H^+ flux for both species. All concentrations tested ($5-10\,\mu M$) caused a significant increase in peak and postexposure steady state O_2/H^+ flux. After an average of 4 h, O_2/H^+ flux for *N. europaea* and *P. aeruginosa* decreased to 50% and 20%, respectively, of pre-exposure levels, but did not reduce below these levels within 12 h.

The average diffusion time for CCCP, KCN, rotenone, and DNP (1.9 ± 0.2 min) was significantly shorter than the time for $CdCl_2$ and PCP (3.9 ± 0.4 min). This difference is likely due to the relatively low solubility (and molecular diffusion coefficient) of $CdCl_2$ and PCP relative to the other toxins (*48, 49*) (SI Table S2). Although experiments were conducted at different temperatures for *N. europaea* (25 °C) and *P. aeruginosa* (37 °C), no significant difference was noted in the time required for diffusion into the biofilm for all toxins tested. Depending on the type of toxin and concentration, diffusion (i.e., penetration) time has been shown to vary considerably (ca. 2−240 min) (*50, 17*). Some toxins/antibiotics (e.g., fluoroquinolones) have been shown to readily penetrate biofilms, while others antibiotics (e.g., glycosides) have a slower penetration time due to complexation with polymeric material (*51*). All of the toxins used in this study penetrated the biofilm within 4 min, and peak physiological stress response occurred within 9 min, followed by a postexposure steady state response after 8−14 min. The biofilms were not significantly different in thickness (average *N. europaea* and *P. aeruginosa* thickness were $99 \pm 19\,\mu m$, and $85 \pm 7\,\mu m$, respectively) ($p = 0.041$, $\alpha = 0.05$). However, the ratio of cells-to-EPS and type of EPS may have varied between the two species of biofilms considerably.

Following diffusion of toxins into biofilms (2−4 min), a peak stress response (increase of O_2 and/or H^+ flux) was observed, followed by a reduction to a postexposure steady state. The time required for peak physiological stress response for CCCP, KCN, rotenone and DNP at all concentrations (5.4 ± 0.4 min) was significantly shorter than the average peak response time for $CdCl_2$ and PCP (7.5 ± 0.5 min), although $CdCl_2$ and PCP had a pronounced long-term effect in 12 h experiments. Based on the time required to re-establish steady state flux, CCCP and DNP (14.2 ± 0.5) also caused long-term effects on respiration, although the bacteria recovered to near-basal levels (indicating acclimation below concentrations of 40 μM). In the following section, the physiological implications of changes in O_2/H^+ flux are discussed in detail.

Discussion

The bacteria respirome is complex, and cells have a wide array of physiological defense mechanism for survival (e.g., efflux pumps, facultative electron transport) (*29, 39*). Bacteria are more resistant to chemical stress following acclimation, and species such as *P. aeruginosa* are able to survive in the presence of some chemical toxins (*50*). Dynamics of homeostatic H^+ transport/cytoplasmic pH regulation in bacteria depend on many factors (e.g., local microenvironment, species type, mode of energy transport), and oxygen transport is complicated by facultative respiration (*29, 52*). These complex transport phenomena make real time monitoring of bioreactor performance using bulk liquid pH and oxygen concentrations difficult. Thus, detailed characterization of bulk liquid-biofilm physiological H^+/O_2 transport will improve our understanding of data collected from real time bulk liquid monitoring, and will aid in development of dynamic simulation models.

Although the time associated with the observed physiological stress response was similar, the mode of action varied

for control drugs (CCCP and KCN) and environmental toxins (rotenone, DNP, CdCl$_2$, and PCP). CCCP (20–40 μM) demonstrated proton ionophore effects for *N. europaea* and *P. aeruginosa* biofilms, and sessile cells subsequently returned to a near-basal physiological respiratory state. This return to basal state is reflective of the enhanced resistance of biofilms to toxins, as CCCP concentrations as low as 20 μM have been shown to completely inhibit metabolic activity in planktonic *N. europaea* (*53*). At the concentrations used in these experiments, KCN inhibited aerobic respiration, and caused cell lysis (verified using membrane integrity stains). *Pseudomonas* spp. are capable of oxidizing CN salts via cyanide monooxygenase (*54*), and are also known to synthesize CN (*55*); therefore preliminary experiments were carried out to ensure that 10 mM KCN was sufficient for inducing cell death in the time allotted for the experiments. Although *N. europaea* cells were not likely to be viable, dormancy of microniche *P. aeuruginosa* populations within the biofilm matrix cannot be excluded (examination with a 100X objective during confocal microscopy analysis supported this conclusion). However, this set of experiments was designed to characterize real time stress responses associated with O$_2$/H$^+$ flux using noninvasive techniques.

Rotenone (25–50 μM) caused a temporary increase (peak stress response) in O$_2$ influx, but had no significant effect on H$^+$ flux. After approximately 8–10 min, O$_2$ flux returned to near basal levels (<3% change). The effect on *N. europaea* was significantly larger than the effect on *P. aeruginosa* cells, which is a reflection of the different innate defense mechanisms (or lack thereof) used by the two species for survival; this may have also been due to the difference in EPS between the two species. Rotenone concentrations of 80 μM have been shown to affect electron transport in planktonic *Nitrobacter* spp. (*56*) and *Pseudomonas* spp. (*57*), though no results were reported for *Nitrosomonas* spp. Based on the known MOA of rotenone, this stress response was likely linked to temporary inhibition of NADH-ATP conversion, which was overcome after a short acclimation period.

No results concerning the exposure of sessile cells to DNP have been reported, although studies using respirometry reported no immediate change in metabolism of planktonic *N. europaea* exposed to 100 μM to 5 mM DNP (*53*), and no measurable effect on planktonic *P. aeruginosa* respiration below 266 μM DNP (*37*). Likewise, one would not expect sessile bacteria to respond to concentrations of DNP below these values. However, DNP (20–40 μM) caused significant uncoupling of O$_2$/H$^+$ transport from ATP synthase within 5.5 ± 0.5 min, and the magnitude of the stress response was not statistically different from CCCP ($p = 0.02$, $\alpha = 0.05$). As expected, the proton ionophore had a more significant effect on H$^+$ flux than O$_2$ flux. We attribute this discrepancy reported in physiological stress responses to the phase-sensitive removal of background signal artifact not associated with O$_2$/H$^+$ transport (*26, 22*). Although it was assumed that no significant DNP degradation (nitrite liberation) (*58*) occurred within the time period of the data reported in Figure 4, rapid acclimation likely occurred after 20 min.

CdCl$_2$ significantly increased O$_2$/H$^+$ flux for both species at the lowest concentration tested (5 μM), followed by a slight reduction in peak flux to postexposure steady state values. At the highest concentration tested (50 μM), CdCl$_2$ caused pronounced oxidative stress for *P. aeruginosa*. Aerobic respiration was inhibited for *N. europaea*, indicating this species was not capable of overcoming this oxidative stress within 12 h. This prolonged oxidative stress may have caused damage sufficient for inhibition of facultative (anaerobic) respiration, which has been shown for planktonic *Pseudomonas* spp. following exposure to 25 μM Cd(II) (*59*). This oxidative stress is not surprising, as Cd(II) has been shown to significantly decrease growth rate of planktonic *P. aerugi-*

nosa (0.2–5.0 mM) (*38, 60*), and oxygen uptake rate of planktonic *N. europaea* (10 μM) (*39*). Genetic/membrane damage has been shown for planktonic *N. europaea* exposed to 10 μM Cd(II) (*39*). Although damage to DNA and/or phospholipid regulatory systems was not quantified, stress response was detected within an average of 7.1 ± 0.3 min, which can be used as an early indicator of cellular stress which may lead to subsequent genome damage.

Although previous experiments reported significant changes in planktonic *P. aeruginosa* viability and genetic regulation following exposure to PCP (37–150 μM), significant changes in substrate/oxygen uptake were not reported (*29*). In this work, significant stress (likely oxidative damage) occurred approximately 8 min after addition of PCP (5–10 μM) for both species. In fact, PCP caused the largest peak increase in O$_2$ flux relative to all other toxins. Post-exposure steady state was significantly lower than the peak stress response, although both species remained in this stressed state for up to 12 h. Neither species has the capability to degrade PCP, so acclimation is unlikely.

Comparison of SR O$_2$/H$^+$ flux data and surface O$_2$ concentration and pH (Figure 3) clearly demonstrate the enhanced temporal resolution and sensitivity of the noise filtering technique (i.e., magnitude *and* direction of O$_2$/H$^+$ transport as opposed to concentration only). This signal filtering effect is due to phase sensitive detection, whereby use of a single microsensor ensures that signal noise is common to the two measurement positions. Although O$_2$ flux may be sufficient for quantifying respiration in some applications (*25*), the multianalyte approach demonstrated here is necessary for monitoring biofilm respiration. This technique can easily be combined with the large data available using other techniques (e.g., transcriptome analysis (*29*), fluorescent in situ hybridization (*39*), and flow cytometry (*61*)) to improve our understanding of time-resolved signaling in biofilms during chemical toxin exposure.

Physiological changes are often the earliest events in cellular stress response (e.g., changes in respiration/growth rate/homeostasis), and many of these mechanisms are utilized by the cells to protect the genome/proteome from damage. Linking the biochemical mechanisms associated with physiological stress response to bulk liquid water quality is critical to the establishment of real time monitoring/control systems. Combining measurements of physiological stress response with parallel genomic/proteomic analysis will be extremely valuable tools for determining if changes in physiological transport are linked to global changes in cell viability (genetic damage, mutation) during exposure to environmental toxins.

Supporting Information Available

Tables S1 and S2; Figures S1–S3. This material is available free of charge via the Internet at http://pubs.acs.org.

Literature Cited

(1) Stewart, P. S.; Costerton, J. W. Antibiotic resistance of bacteria in biofilms. *Lancet.* **2001**, *358*, 135–138.
(2) Elasri, M. O.; Miller, R. V. Study of the response of a biofilm bacterial community to UV radiation. *Appl. Environ. Microbiol.* **1999**, *65*, 2025–2031.
(3) Ma, M.; Eaton, J. W. Multicellular oxidant defense in unicellular organisms. *Proc. Nat. Acad. Sci. U.S.A.* **1992**, *89*, 7924–7928.
(4) Davey, M. E.; O'Toole, G. A. Microbial biofilms: From ecology to molecular genetics. *Microbiol. Mol. Biol. Rev.* **2000**, *64*, 847–867.
(5) Christensen, B. B.; Sternberg, C.; Andersen, J. B.; Eberl, L.; Moller, S.; Givskov, M.; Molin, S. Establishment of new genetic traits in a microbial biofilm community. *Appl. Environ. Microbiol.* **1998**, *64*, 2247–2255.
(6) Wang, R.; Terada, A.; Lackner, S.; Smets, B. F.; Henze, M.; Xia, S.; Zhao, J. Nitritation performance and biofilm development of co- and counter-diffusion biofilm reactors: model-

ing and experimental comparison. *Water Res.* **2009**, *43*, 2699–2709.

(7) Satoh, H.; Ono, H.; Rulin, B.; Kamo, J.; Okabe, S.; Fukushi, K. I. Macroscale and microscale analyses of nitrification and denitrification in biofilms attached on membrane aerated biofilm reactors. *Water Res.* **2004**, *38*, 1633–1641.

(8) Smith, D. P.; Rector, T.; Reid-Black, K.; Hummerick, M.; Strayer, R.; Birmele, M.; Roberts, M. S.; Garland, J. L. Redox control bioreactor: A unique biological water processor. *Biotechnol. Bioeng.* **2008**, *99*, 830–845.

(9) Liao, B. Q.; Zheng, M. R.; Ratana-Rueangsri, L. Treatment of synthetic kraft evaporator condensate using thermophilic and mesophilic membrane aerated biofilm reactors. *Water Sci. Technol.* **2010**, *61*, 1749–1756.

(10) Semmens, M. J.; Dahm, K.; Shanahan, J.; Christianson, A. COD and nitrogen removal by biofilms growing on gas permeable membranes. *Water Res.* **2003**, *37*, 4343–4350.

(11) Heffernan, B.; Murphy, C. D.; Syron, E.; Casey, E. Treatment of fluoroacetate by a *Pseudomonas fluorescens* biofilm grown in membrane aerated biofilm reactor. *Environ. Sci. Technol.* **2009**, *43*, 6776–6785.

(12) Casey, E.; Glennon, B.; Hamer, G. Review of membrane aerated biofilm reactors. *Resour. Conserv. Recycl.* **2000**, *27*, 203–215.

(13) Puig, S.; Corominas, L.; Traore, A.; Colomer, J.; Balaguer, M. D.; Colprim, J. An on-line optimization of a SBR cycle for carbon and nitrogen removal based on on-line pH and OUR: The role of dissolved oxygen control. *Water Sci. Technol.* **2006**, *53*, 171–178.

(14) Ndegwa, P. M.; Wang, L.; Vaddella, V. K. Potential strategies for process control and monitoring of stabilization of dairy wastewaters in batch aerobic treatment systems. *Process. Biochem.* **2007**, *42*, 1272–1278.

(15) Bishop, P. L.; Yu, T. A. Microelectrode study of redox potential change in biofilms. *Water Sci. Technol.* **1999**, *39*, 179–185.

(16) Chandran, K.; Love, N. G. Physiological state, growth mode, and oxidative stress play a role in Cd(II)-mediated inhibition of *Nitrosomonas europaea* 1971. *Appl. Environ. Microbiol.* **2008**, *74*, 2447–2453.

(17) Jang, A.; Szabo, J.; Hosni, A. A.; Coughlin, M.; Bishop, P. L. Measurement of chlorine dioxide penetration in dairy process pipe biofilms during disinfection. *Appl. Microbiol. Biotechnol.* **2006**, *72*, 368–376.

(18) Choi, O.; Hu, Z. Size dependent and reactive oxygen species related nanosilver toxicity to nitrifying bacteria. *Environ. Sci. Technol.* **2008**, *42*, 4583–4588.

(19) Villez, K.; Rosen, C.; Anctil, F.; Duchesne, C.; Vanrolleghem, P. A. Qualitative representation of trends: an alternative approach to process diagnosis and control. *Water Sci. Technol.* **2008**, *57*, 1525–1532.

(20) Belia, E.; Amerlinck, Y.; Benedetti, L.; Johnson, B.; Sin, G.; Vanrolleghem, P. A.; Gernaey, K. V.; Gillot, S.; Neumann, M. B.; Rieger, L.; Shaw, A.; Villez, K. Wastewater treatment modelling: dealing with uncertainties. *Water Sci. Technol.* **2009**, *60*, 1929–1941.

(21) Syron, E.; Casey, E. Membrane-aerated biofilms for high rate biotreatment: Performance appraisal, engineering principles, scale-up, and development requirements. *Environ. Sci. Technol.* **2008**, *42*, 1833–1844.

(22) Porterfield, D. M. Measuring metabolism and biophysical flux in the tissue, cellular and sub-cellular domains: Recent developments in self-referencing amperometry for physiological sensing. *Biosens. Bioelectron.* **2007**, *22*, 1186–1196.

(23) McLamore, E. S.; Mohanty, S.; Shi, J.; Rickus, J. L.; Porterfield, D. M. Real time neuronal glutamate flux during potassium stimulation. *J. Neurosci. Methods* **2010**, *189*, 14–22.

(24) Porterfield, D. M.; Smith, P. J. S. Single-cell, real-time measurements of extracellular oxygen and proton fluxes from *Spirogyra grevilleana*. *Protoplasma* **2000**, *212*, 80–88.

(25) Sanchez, B. C.; Ochoa-Acuña, H.; Porterfield, D. M.; Sepúlveda, M. S. Oxygen flux as an indicator of physiological stress in fathead minnow (*Pimephales promelas*) embryos: A realtime biomonitoring system of water quality. *Environ. Sci. Technol.* **2008**, *42*, 7010–7017.

(26) McLamore, E. S.; Porterfield, D. M.; Banks, M. K. Non-invasive self-referencing electrochemical sensors for quantifying real time biophysical flux in biofilms. *Biotechnol. Bioeng.* **2009**, *102*, 791–799.

(27) Bard, A. J.; Faulkner, L. R. *Electrochemical Methods: Fundamentals and Applications*, 2nd ed.; Wiley: New York, 2000.

(28) Costa, E.; Pérez, J.; Kreft, J. U. Why is metabolic labour divided in nitrification. *Trends Microbiol.* **2006**, *14*, 213–219.

(29) Muller, J. F.; Stevens, A. M.; Craig, J.; Love, N. G. Transcriptome analysis reveals that multidrug efflux genes are upregulated to protect *Pseudomonas aeruginosa* from pentachlorophenol stress. *Appl. Environ. Microbiol.* **2007**, *73*, 4550–4558.

(30) McLamore, E. S.; Morse, A.; Jackson, W. A. Abiotic transport in a membrane aerated bioreactor. *J. Membr. Sci.* **2007**, *298*, 110–116.

(31) Chatni, M. R.; Maier, D. E.; Porterfield, D. M. Evaluation of microparticle materials for enhancing the performance of fluorescent lifetime based optrodes. *Sens. Actuators B* **2009**, *141*, 471–477.

(32) Lee, S. K.; Okura, I. Photostable optical oxygen sensing material: Platinum tetrakis(pentafluorophenyl)porphyrin immobilized in polystyrene. *Anal. Comm.* **1997**, *34*, 185–188.

(33) Chatni, M. R.; Porterfield, D. M. Self-referencing optrode technology for non-invasive real-time measurement of biophysical flux and physiological sensing. *Analyst* **2009**, *134*, 2224–2232.

(34) Porterfield, D. M.; McLamore, E. S.; Banks, M. K. Microsensor technology for measuring for measuring H^+ flux in buffered media. *Sens. Actuators B* **2009**, *136*, 383–387.

(35) Mitchell, P. Coupling of phosphorylation to electron and hydrogen transfer by a chemiosmotic type of mechanism. *Nature.* **1961**, *191*, 144–148.

(36) Hatcher, J. M.; Pennell, K. D.; Miller, G. W. Parkinson's disease and pesticides: a toxicological perspective. *Trends Pharmacol. Sci.* **2008**, *29*, 322–329.

(37) Ray, S.; Peters, C. A. Changes in microbiological metabolism under chemical stress. *Chemosphere.* **2008**, *71*, 474–483.

(38) Priester, J. H.; Stoimenov, P. K.; Mielke, R. E.; Webb, S. M.; Ehrhardt, C.; Zhang, J. P.; Stucky, G. D.; Holden, P. A. Effects of soluble cadmium salts versus CdSe quantum dots on the growth of planktonic *Pseudomonas aeruginosa*. *Environ. Sci. Technol.* **2009**, *43*, 2589–2594.

(39) Chandran, K.; Love, N. G. Physiological state, growth mode, and oxidative stress play a role in Cd(II)-mediated inhibition of *Nitrosomonas europaea* 1971. *Appl. Environ. Microbiol.* **2008**, *74*, 2447–2453.

(40) Escher, B. I.; Hunziker, R.; Schwarzenbach, R. P. Kinetic model to describe the intrinsic uncoupling activity of substituted phenols in energy transducing membranes. *Environ. Sci. Technol.* **1999**, *33*, 560–570.

(41) Drinking Water Standards and Health Advisories, 822-R-06-01; U.S. EPA Office of Water: Washington, DC, 2006.

(42) de Beer, D.; van den Heuvel, J. C.; Ottengraf, S. P. P. Microelectrode measurements of the activity distribution in nitrifying bacterial aggregates. *Appl. Environ. Microbiol.* **1993**, *59*, 573–579.

(43) de Beer, D.; Schramm, A.; Santegoeds, C. M.; Kuhl, M. A nitrite microsensor for profiling environmental biofilms. *Appl. Environ. Microbiol.* **1997**, *63*, 973–977.

(44) Bishop, P.; Yu, T. A microelectrode study of redox potential change in biofilms. *Water Sci. Technol.* **1999**, *39*, 179–185.

(45) Lee, J. H.; Seo, Y.; Lim, T. S.; Bishop, P. L.; Papautsky, I. MEMS needle-type sensor array for in situ measurements of dissolved oxygen and redox potential. *Environ. Sci. Technol.* **2007**, *41*, 7857–7863.

(46) Spycher, S.; Smejtek, P.; Netzeva, T. I.; Escher, B. I. Toward a class-independent quantitative structure-activity relationship model for uncouplers of oxidative phosphorylation. *Chem. Res. Toxicol.* **2008**, *21*, 911–927.

(47) Ozaki, S.; Kano, S.; Shirai, O. Electrochemical elucidation on the mechanism of uncoupling caused by hydrophobic weak acids. *Phys. Chem. Physics.* **2008**, *10*, 4449–4455.

(48) Schwarzenbach, R. P., Gschwend, P. M.; Imboden, D. M. *Environmental Organic Chemisry*, 2nd ed.; John Wiley & Sons, Inc.: Danvers, MA, 2003, 61−68.

(49) Zhu, R.; Macfie, S. M.; Ding, Z. Cadmium-induced plant stress investigated by scanning electrochemical microscopy. *J. Exp. Bot.* **2005**, *56*, 2831–2838.

(50) Ander, J. N.; Franklin, M. J.; Stewart, P. S. Role of antibiotic penetration limitation in *Klebsiella pneumoniae* biofilm resistance to ampicillin and ciprofloxacin. *Antimicrob. Agents Chemother.* **2000**, *44*, 1818–1824.

(51) Parsek, M. R.; Fuqua, C. Biofilms 2003: Emerging themes and challenges in the study of surface-associated microbial life. *J. Bacteriol.* **2004**, *186*, 4427–4440.

(52) Booth, I. R. Regulation of cytoplasmic pH in bacteria. *Microbiol. Rev.* **1985**, *49*, 359–378.

(53) Schmidt, I.; Look, C.; Bock, E.; Jetten, M. S. M. Ammonium and hydroxylamine uptake and accumulation in *Nitrosomonas*. *Microbiol.* **2004**, *150*, 1405–1412.

(54) Akcil, A.; Mudder, T. Microbial destruction of cyanide wastes in gold mining: Process review. *Biotechnol. Lett.* **2003**, *25*, 445–450.

(55) Zlosnik, J. E. A.; Tavankar, G. R.; Bundy, J. G.; Mossialos, D.; O'Toole, R.; Williams, H. D. Investigation of the physiological relationship between the cyanide-insensitive oxidase and cyanide production in *Pseudomonas aeruginosa. Microbiology.* **2006**, *152*, 1407–1415.

(56) Sundermeyer, H.; Bock, E. Energy metabolism of autotrophically and heterotrophically grown cells of *Nitrobacter winogradskyi. J. Arch. Microbiol.* **1981**, *130*, 250–254.

(57) Lee, J. H.; Gu, M. B. An integrated mini biosensor system for continuous water toxicity monitoring. *Biosens. Bioelectron.* **2005**, *20*, 1744–1749.

(58) Andreozzi, R.; Cesaro, R.; Marotta, R.; Pirozzi, F. Evaluation of biodegradation kinetic constants for aromatic compounds by means of aerobic batch experiments. *Chemosphere.* **2006**, *62*, 1431–1436.

(59) Pagès, D.; Sanchez, L.; Conrod, S.; Gidrol, X.; Fekete, A.; Schmitt-Kopplin, P.; Heulin, T.; Achouak, W. Exploration of intraclonal adaptation mechanisms of *Pseudomonas brassicacearum* facing cadmium toxicity. *Environ. Microbiol.* **2007**, *9*, 2820–2835.

(60) Wang, C. L.; Michels, P. C.; Dawson, S. C.; Kitisakkul, S.; Baross, J. A.; Keaslilng, D.; Clark, D. S. Cadmium removal by a new strain of *Pseudomonas aeruginosa* in aerobic culture. *Appl. Environ. Micobiol.* **1997**, *63*, 4075–4078.

(61) Yarwood, J. M.; Bartels, D. J.; Volper, E. M.; Greenberg, E. P. Quorum sensing in *Staphylococcus* aureus biofilms. *J. Bacteriol.* **2004**, *186*, 1838–1850.

ES1012356